INSTITUTE OF PHYSICS PUBLISHING JOURNAL OF OPTICS A: PURE AND APPLIED OPTICS

J. Opt. A: Pure Appl. Opt. **5** (2003) 47–52 PII: S1464-4258(03)54493-2

Optical properties of bubbles

Alexander A Kokhanovsky

Institute of Environmental Physics, Bremen University, PO Box 330440, Bremen, Germany
and
Institute of Physics, 70 Skarina Avenue, Minsk 220072, Belarus

E-mail: alexk@iup.physik.uni-bremen.de

Received 7 October 2002, in final form 18 November 2002
Published 13 December 2002
Online at stacks.iop.org/JOptA/5/47

Abstract
The intensity and polarization characteristics of light scattered by bubbly media is studied, assuming that the size of bubbles is much larger than the wavelength of the incident light, which is a valid assumption, e.g., for bubbles in water and sea ice. The influence of possible nonsphericity of bubbles, light absorption and multiple light scattering effects is neglected. The dependence of the phase matrix on the relative refractive index of bubbles n is studied in the range $n = 0.3$–0.9. Results presented can be used for the development of analytical models of polarized light propagation in bubbly media, which take into account special features of bubble light scattering.

Keywords: Bubbles, light scattering, geometrical optics, Mie theory

1. Introduction

Optical properties of bubbles are of interest for many applications, including light propagation in oceanic water, ice and various technical media [1–4]. Usually the size of bubbles a is much larger than the wavelength of visible light λ. Then phase function and polarization characteristics are independent of their size everywhere except the forward, backward, and critical scattering regions, where the light diffraction should be taken into account. For spherical bubbles, this can be achieved using the Mie theory [5], which correctly accounts for diffraction effects. Physical optics and complex angular momentum approximations [6–9] can be of help to see the physics behind a diffraction optics phenomena, which otherwise is hidden in the complicated Mie solution.

The main aim of this paper is to study the dependence of the phase matrix of spherical bubbles on their refractive index, assuming that $a \gg \lambda$. The correct way to do this is to use the Mie theory for a given bubble size distribution [5]. We present such results for the case of air bubbles in water, assuming that the effective radius of droplets is equal to 15 and 30 μm.

It is known that geometrical optics can be considered as a limiting case of wave optics as $\lambda \to 0$. Therefore, it is of importance from a general point of view to derive these limiting patterns for elements of the Mueller matrix of bubbly media as $\lambda \to 0$ at various values of the refractive index n. The numerical calculation of these limiting patterns constitutes a major part of this work. This is essentially the extension of work [10], which was performed in the assumption that the relative refractive index of bubbles is 0.75. Only the intensity of scattered light and not a full Mueller matrix was considered in [10].

The modern ray tracing code, used in calculations, is described elsewhere [11]. The physical idea behind the geometrical optics approach, which is the base of code [11], is quite simple: the tracing of the geometrical optics rays as they interact with a bubble surface. The Fresnel equations [10, 11] are used to find the light energy and polarization change at the bubble–host medium interface. Results obtained with code [11] for the intensity of scattered light coincide with those given in [10] at a particular case of $n = 0.75$.

2. Intensity and polarization characteristics of scattered light

The interaction of light with a single bubble can be described in the framework of the Stokes vector formalism [12]. Then the Stokes vector of scattered light $\vec{S}$ is related to the Stokes vector of the incident light $\vec{S}_0$ by a following formula in a linear optics approximation [12]:

$$\vec{S} = \frac{F(\theta)}{k^2 r^2} \hat{p}(\theta) \vec{S}_0, \tag{1}$$

where θ is the scattering angle, $k = 2\pi/\lambda$, r is the distance to the observation point and $F(\theta)$ is the dimensionless scattering

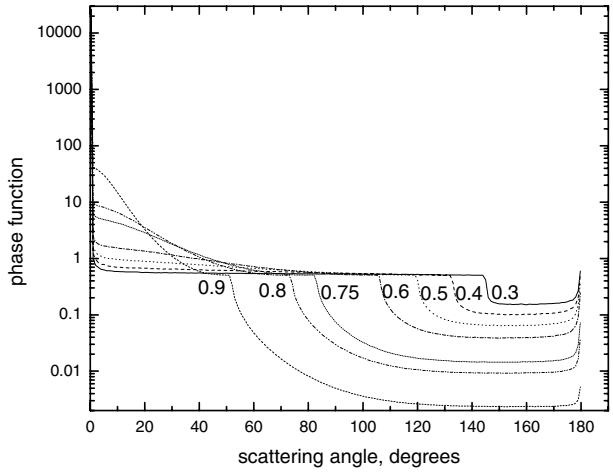

Figure 1. The phase function of bubbles for various $n = 0.3$, 0.4, 0.5, 0.6, 0.75, 0.8, 0.9, obtained in the framework of the geometrical optics.

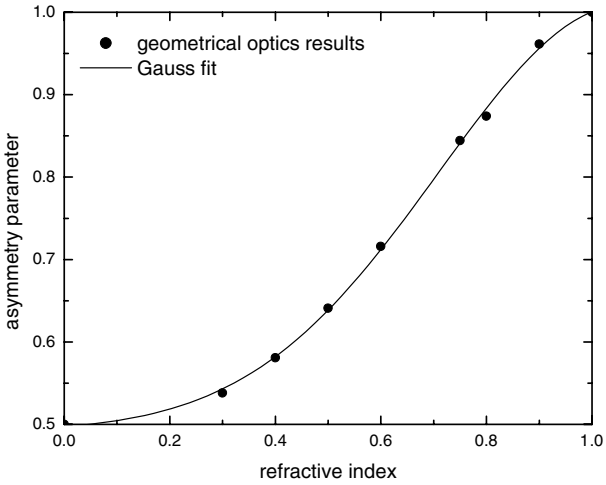

Figure 2. The dependence of the asymmetry parameter g on n, obtained in the geometrical optics approximation (circles). Curve gives the Gauss fit results (see equation (8)).

function, which defines the scattering cross section as [12]

$$C_{sca} = \frac{2\pi}{k^2}\int_0^{\pi} F(\theta)\sin\theta\,\mathrm{d}\theta. \tag{2}$$

The normalized scattering matrix $\hat{p}$, which coincides with the normalized Mueller matrix of the problem at hand, has the following general structure for spheres [12]:

$$\hat{p} = \begin{pmatrix} 1 & p_{12} & 0 & 0 \\ p_{12} & 1 & 0 & 0 \\ 0 & 0 & p_{44} & p_{34} \\ 0 & 0 & -p_{34} & p_{44} \end{pmatrix}. \tag{3}$$

We note that

$$\frac{2\pi}{C_{sca}k^2}\int_0^{\pi} F(\theta)\sin\theta\,\mathrm{d}\theta = 1. \tag{4}$$

In what follows we study not the function $F(\theta)$, but the so-called phase function

$$p(\theta) = \frac{4\pi F(\theta)}{C_{sca}k^2}, \tag{5}$$

which gives a conditional probability of light scattering in a particular direction θ and normalized as follows:

$$\tfrac{1}{2}\int_0^{\pi} p(\theta)\sin\theta\,\mathrm{d}\theta = 1. \tag{6}$$

Due to large size of droplets, the value of C_{sca} is equal to $2S$ [2, 6, 12], where S is the average geometrical cross section of bubbles.

We underline that equation (1) is also valid for spherical polydispersions. Then the function $F(\theta)$, products $F(\theta)p_{ij}$ $(i, j = 1, 2, 3, 4)$ and scattering cross section C_{sca} should be averaged with respect to the bubble size distribution function $f(a)$ [12].

The phase function $p(\theta)$, calculated using the Monte Carlo ray tracing code [11], is given in figure 1 for various relative indices n of monodispersed bubbles ($n = 0.75$ corresponds to the case of air bubbles in water). The geometrical optics calculations were supplemented by the wave optics results at small scattering angles, using the well-known Airy formula [12] ($F(\theta) \sim 4J_1^2(ka\theta)/\theta^2$ as $\theta \to 0$, where J_1 is the Bessel function). We assumed in calculations that the radius of a bubble $a = 1$ mm and $\lambda = 0.55$ μm. So we have $\xi \equiv \frac{a}{\lambda} \approx 1818$, which explains a sharp peak in the forward direction. Its width is proportional to λ/a. As was stated above, $p(\theta)$ does not change with ξ (except at small scattering angles, if the diffraction is taken into account) in the framework of the geometrical optics approach. Thus, results given in figure 1 correspond to the asymptotic scattering regime ($\xi \to \infty$).

The behaviour of phase functions is completely different for angles $\theta < \theta_c$ and $\theta > \theta_c$, where $\theta_c = 2\arccos(n)$ is the so-called critical scattering angle [2, 9]. The value of θ_c grows with $n - 1$. Formally, we have $\theta_c = 0°$ at $n = 1$ and $\theta_c = 180°$ at $n = 0$. It follows at $n = 0.75$, $\theta_c \approx 82.8°$.

In particular, we see that for $n = 0.3$ the phase function is almost constant in the region of scattering angles smaller than approximately 140° (with the exception of the diffraction zone at small angles). It sharply decreases at $\theta = \theta_c \approx 145°$. The phase function is again almost constant at $\theta > 145°$ (except as $\theta \to 180°$, which is due to the axial focusing effect [5]). Similar behaviour is observed for other n (see figure 1). Generally, the sharpness of the step at $\theta = \theta_c$ increases with $\Delta n = 1 - n$. The phase function $p(\theta)$ coincides with the delta function $\delta(\theta)$ at $n = 1$. It is given by a combination of the Airy diffraction pattern at small angles and an isotropic part outside of the diffraction peak at $n = 0$. This is due to the fact that waves do not penetrate inside a particle in this case.

The forward–backward asymmetry of phase functions is usually represented by the asymmetry parameter [12]

$$g = \tfrac{1}{2}\int_0^{\infty} p(\theta)\sin\theta\cos\theta\,\mathrm{d}\theta. \tag{7}$$

This parameter is given in table 1 and figure 2 for various n. We see that g increases as $n \to 1$. The solid curve gives a fit,

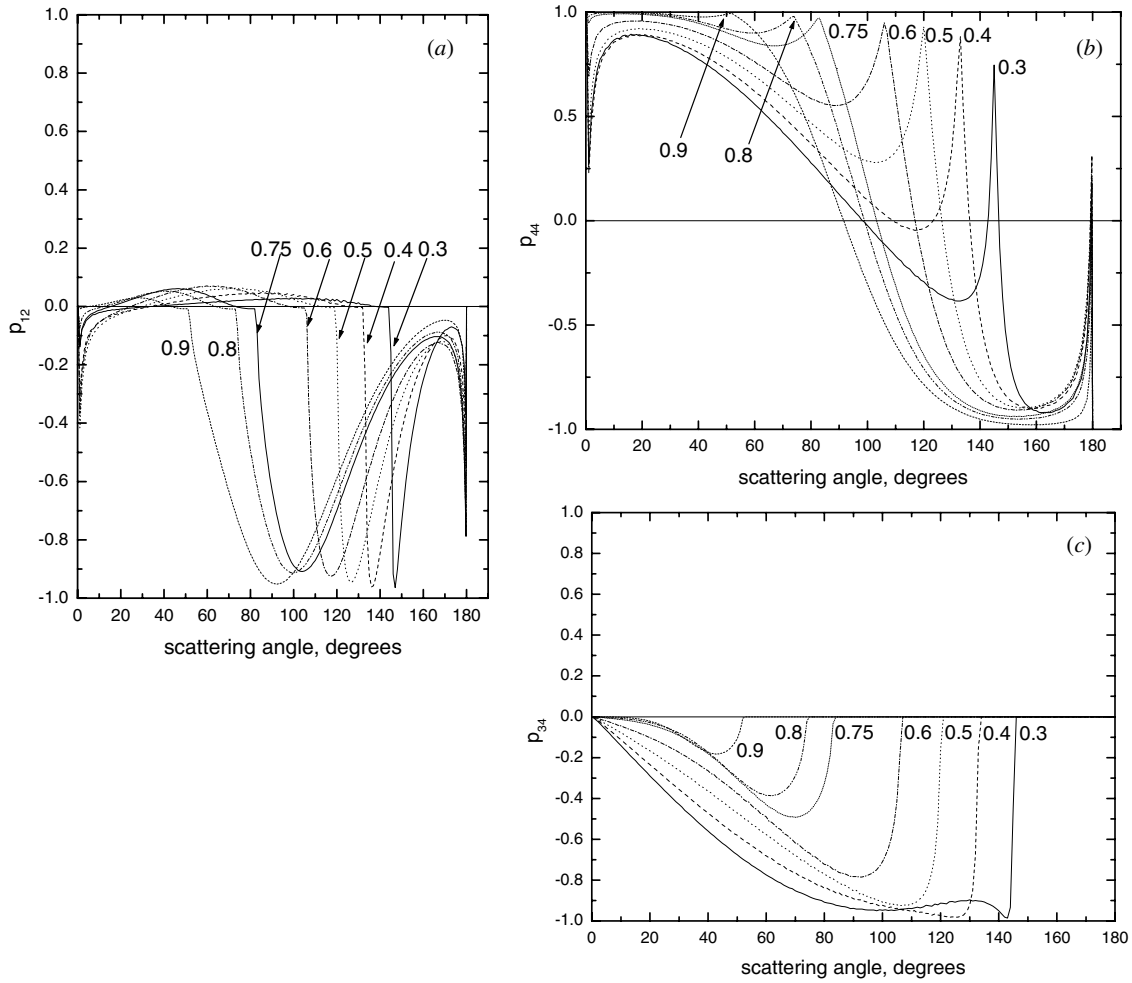

Figure 3. As in figure 1, but for p_{12} (a), p_{44} (b), p_{34} (c).

using the Gaussian distribution

$$g = g_0 + \frac{A}{\Delta\sqrt{\pi/2}} \exp\left\{-2\left(\frac{n-n_0}{\Delta}\right)^2\right\}, \qquad (8)$$

where $g_0 = 0.492\,74$, $n_0 = 1.048\,82$, $\Delta = 0.692\,33$, and $A = 0.444\,66$. Note that the parameter g determines reflectance $r = 1 - t$ and transmittance t of optically thick bubbly layers [12]. In particular, we have for the large optical thickness τ of a bubbly medium [12]

$$t = \frac{1}{1.07 + 0.75\tau(1-g)}. \qquad (9)$$

Bubbly media with the same values of $\tau(1-g)$ have close values of r and t as $\tau \to \infty$, despite having quite different single scattering laws (see figure 1).

The elements p_{12}, p_{44}, p_{34} of the matrix $\hat{p}$, given by equation (3), are presented in figures 3(a)–(c). The element p_{12} (see figure 3(a)) is equal (with opposite sign) to the degree of linear polarization p_l of scattered light, assuming that the incident light is unpolarized. Therefore, we see that p_l is mostly positive (the oscillations of the electric vector are in the plane perpendicular to the scattering plane, containing incident and scattered beams). The degree of linear polarization sharply increases at the critical scattering angle. Then it takes a maximum and again decreases for larger scattering angles. The maximum is sharper for smaller n. Note that there is also an increase in the degree of linear polarization in the vicinity of the backscattering direction. Also, we have $p_l(0) = p_l(\pi) = 0$ for all n. This suggests that there is no light depolarization in the forward and backward scattering directions for spherical bubbles.

The element p_{44}, presented in figure 3(b), gives the degree of circular polarization p_c of scattered light, assuming that incident light is right-hand circularly polarized ($p_c = 1$). In particular, we see that $p_c = -1$ for scattered light at exactly the backward direction for arbitrary n. This is due to the conservation of rotation sense (photon angular momentum)

Table 1. The asymmetry parameter g for various n.

n	g
0.0	0.5
0.3	0.5380
0.4	0.5807
0.6	0.7160
0.75	0.8443
0.8	0.8869
0.9	0.9614
1.0	1.0

in the light backscattering by bubbles (and spheres in general). Generally, light scattering by bubbles reduces the circular polarization of incident circularly polarized light ($|p_c| \leqslant 1$). In particular, the value of p_c is equal to zero for four scattering angles at $n = 0.3$ (see figure 3(b)). The strong variation of p_c is observed near the backward direction. For air bubbles in water ($n = 0.75$) p_c varies very little with $\theta < \theta_c$. However, it drops sharply at the critical angle, reversing the sign of p_c around $\theta \approx 105°$. Therefore, the scattering process at angles larger than 105° for air bubbles in water transforms incident right-hand polarized light to a left-hand circularly polarized mode.

The element p_{34}, presented in figure 3(c), gives the value of p_c for the case of linearly polarized incident light with the azimuth −45°. We see that the value of p_c is equal to zero at $\theta > \theta_c$. Therefore, linearly polarized light cannot be transformed in a circularly polarized mode at $\theta > \theta_c$ in the geometrical optics scattering regime.

Following this brief discussion of various matrix elements, we would like to underline that data given in figures 1 and 3 (in combination with equation (1)) can be used to study the interaction of arbitrarily polarized light beams with bubbly media in the framework of the single scattering approximation, assuming that $\lambda/a \to 0$ [6].

It is interesting to see how the geometrical optics results described above correspond to the wave optics results. For this, we have presented the comparison of geometrical optics [11] and Mie [5] calculations at $n = 0.75$, $\lambda = 0.55$ μm in figures 4(a)–(d). Geometrical optics curves in figures 4(a)–(d) (solid curves) coincide with those given in figures 1 and 3 at $n = 0.75$. The bubble size distribution in Mie calculations was assumed to be

$$f(a) = Aa^6 \exp(-9a/a_{ef}), \tag{10}$$

where a is the radius of droplets and A = constant. The function $f(a)$ is normalized as follows [12]:

$$\int_0^\infty f(a)\,\mathrm{d}a = 1. \tag{11}$$

We have used two values of the effective radius a_{ef}, namely 15 and 30 μm, in Mie calculations.

It follows from figure 4(a) that phase functions calculated using geometrical optics and wave optics differ considerably around $\theta \approx \theta_c$ (and in the diffraction zone, which is mostly due to different size of bubbles used in wave and geometrical optics calculations). They depend on the size of particles and wavelength in the region of critical scattering [6–9]. This dependence is totally absent in the framework of the geometrical optics description [9]. We see that the scattering angle corresponding to the maximum of scattering in the critical scattering region increases with $\rho_{ef} = 2\pi a_{ef}/\lambda$. Its position approaches the asymptotic value as $\rho_{ef} \to \infty$. The wavelength dependence produces coloured rings in scattered light around $\theta \approx \theta_c$ if one uses white light illumination. Red light with larger λ (smaller ρ_{ef}) gives a maximum at smaller θ as compared with blue light for the same bubble size distribution (see figure 4(a)). The intensity of red rings is expected to be larger than blue ones. On the other hand, the critical scattering of a monochromatic light (e.g., laser) can be used to estimate the value of a_{ef} [7]. Note that coloured rings in white light scattering patterns for bubbly media have been observed experimentally [13, 14].

It follows from figure 4(a) that the geometrical optics has a high accuracy in the backward hemisphere ($\theta \geqslant 90°$) for air bubbles in water at ρ_{ef} larger than 180. The corresponding limiting value of ρ_{ef} for water droplets in air is larger (around 1000 [15]). This is due to the rainbow effect [15], which cannot be described by a geometrical optics alone.

The rainbow effect does not exist for bubbles, however. Therefore, main errors of the geometrical optics for small bubbles are in the vicinity of the critical ($\theta \approx 82.8°$) and glory ($\theta \approx 180°$) scattering regions, where the diffraction of light should be properly taken into account. The discrepancy around small scattering angle ($\theta \approx 0°$) is mostly due to different values of the bubble radii assumed in the geometrical optics and Mie calculations.

A close examination of figures 4(b)–(d) shows generally the same features as we found in figure 4(a). Namely, major differences arise in the vicinity of the critical and glory [6–9] scattering regions. The dependence of p_{12}, p_{34}, and p_{44} on a_{ef} can be used for bubble optical sizing.

It is interesting that the position and the value of the maximal polarization (see figure 4(b)) is described by the geometrical optics method with a high accuracy. This feature can be applied to measurements of the refractive index of a host medium with spherical air inclusions.

3. Conclusion

We have studied here the dependence of the normalized matrix elements p_{12}, p_{34}, p_{44} and the phase function $p(\theta)$ on the relative refractive index of bubbles with sizes much larger than the wavelength of incident light. The possible light absorption, multiple light scattering and change of frequency during the scattering process is neglected. We also ignored the possible distortion of droplet shape [16, 17] and the presence thin organic films, which can be formed on the surface of bubbles in many cases [14, 18]. These assumptions allowed us to derive an idealized geometrical optics pattern picture, which can be further clarified, if needed, to account for additional factors (e.g., using Mie theory).

Note that bubbles can be air trapped in various materials. The medium of particular importance is, of course, ocean. In particular, oceanic whitecaps play an important role in the air–ocean exchange processes, modification of the planetary albedo and satellite remote sensing (as an obstacle for an accurate determination of aerosol optical thickness and chlorophyll concentration from orbiting satellites) [19]. It should be stressed that results obtained are generally applicable to any spherical particle having refractive index smaller than that of a surrounding medium (e.g. water droplets or bio-particles trapped in glass or various solids).

The matrix (3) plays a fundamental role in the vector radiative transfer in multiple light scattering media [12, 20]. It can be used, therefore, to facilitate the derivation of analytical results in the field of polarized multiple light scattering, taking into account the peculiarities of single light scattering by particles with $n < 1$, considered here.

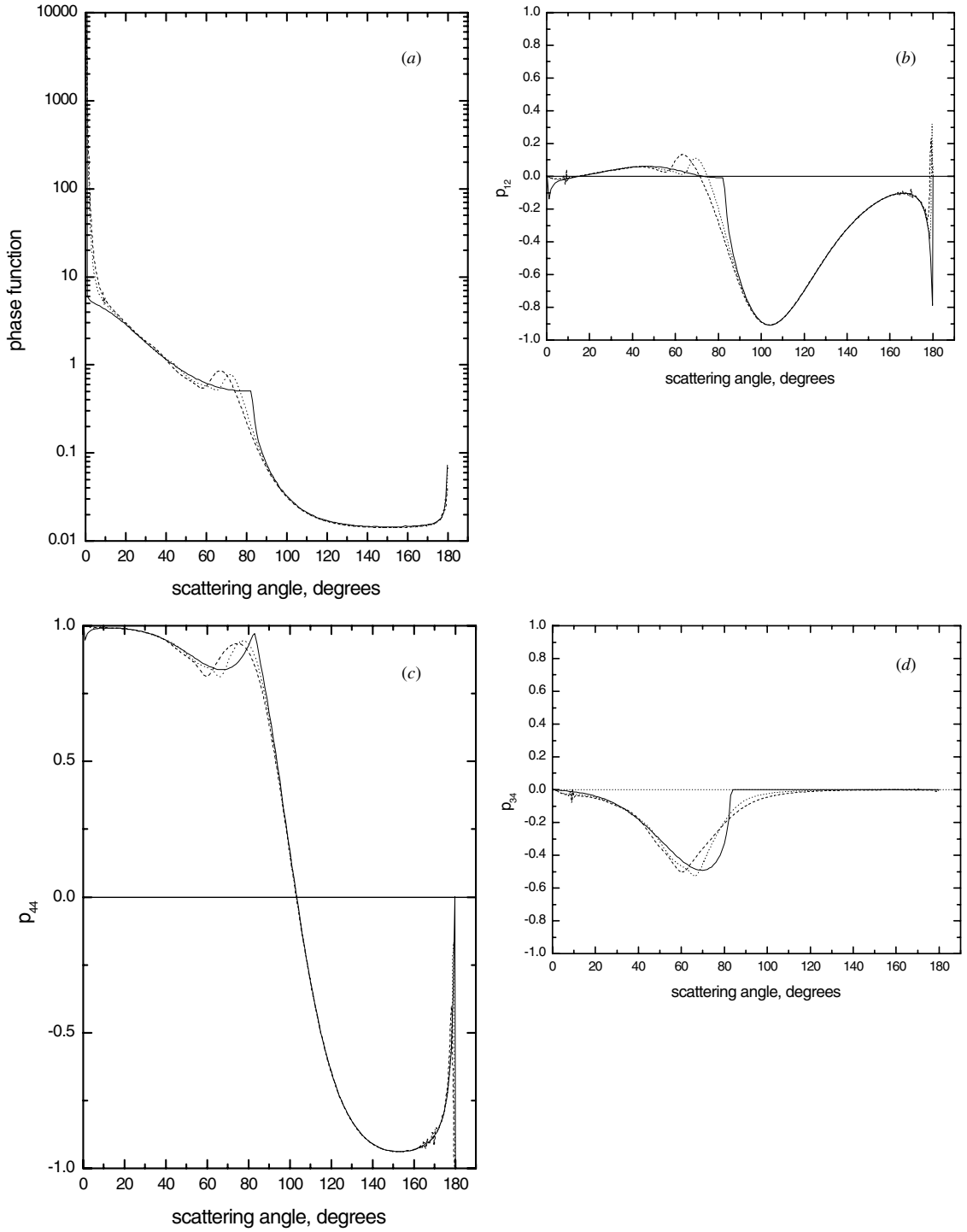

Figure 4. (*a*) As in figure 1, but at $n = 0.75$ only (solid curves). Dashed curves give the Mie theory results for air bubbles in water, having the size distribution (10) with a_{ef} equal to 15 μm (long-dashed curve) and 30 μm (short-dashed curve). The wavelength is equal to 0.55 μm. (*b*) As in (*a*) except for p_{12}. (*c*) As in (*a*) except for p_{44}. (*d*) As in (*a*) except for p_{34}.

We underline that the critical scattering region can be used for optical bubble sizing [7]. This could be a useful addition to small-angle particle sizing methods [12].

Acknowledgments

This work was supported by the Institute of Environmental Physics (Bremen University). The author is grateful to A Macke for providing his Monte Carlo ray tracing code [11].

References

[1] Baldy S 1988 Bubbles in the close vicinity of breaking waves: statistical characteristics of the generation and dispersion mechanism *J. Geophys. Res.* C **93** 8239–48

[2] Kokhanovsky A 1988 Integral scattering characteristics of light scattering by spherical inclusions with relative refractive index below unity *Opt. Spectrosc. (USSR)* **67** 93–5

[3] Flatau P *et al* 2000 Remote sensing of bubble clouds in sea water *Q. J. R. Meteorol. Soc.* **126** 2511–23

[4] Yan B *et al* 2002 Role of oceanic air bubbles in atmospheric correction of ocean color imagery *Appl. Opt.* **41** 2202–12
[5] Kerker M 1969 *The Scattering of Light and Other Electromagnetic Radiation* (New York: Academic)
[6] Marston P L *et al* 1982 Light scattering by bubbles in liquids: Mie theory, physical-optics approximations, and experiments *Appl. Sci. Res.* **38** 373–83
[7] Langley D S and Marston P L 1984 Critical-angle scattering of laser light from bubbles in water: measurements, models, and application to sizing of bubbles *Appl. Opt.* **23** 1044–54
[8] Langley D S and Marston P L 1991 Forward glory scattering from bubbles *Appl. Opt.* **30** 3452–8
[9] Fiedler-Ferrari N *et al* 1991 Theory of near-critical-angle scattered from a curved interface *Phys. Rev.* A **43** 1005–38
[10] Davis G E 1952 Scattering of light by an air bubble in water *J. Opt. Soc. Am.* **45** 572–81
[11] Macke A 2000 Monte Carlo calculations of light scattering by large particles with multiple internal inclusions *Light Scattering by Nonspherical Particles* ed M I Mishchenko, J W Hovenier and L D Travis (New York: Academic) pp 309–22
[12] Kokhanovsky A A 2001 *Light Scattering Media Optics: Problems and Solutions* (Chichester: Springer)
[13] Pulfrich C 1888 Uber eine dem Regenbogen verwandte Erscheinung der Toatalreflexion *Ann Phys. Chem.* **33** 209–12
[14] Marston P L 1990 Colors observed when sunlight is scattered by bubble clouds in seawater *Appl. Opt.* **30** 3479–84
[15] Van de Hulst H C 1981 *Light Scattering by Small Particles* (New York: Dover)
[16] Arnott W P and Marston P L 1988 Optical glory of small freely rising gas bubbles in water: observed and computed cross-polarized backscattering patterns *J. Opt. Soc. Am.* A **5** 496–506
[17] Arnott W P and Marston P L 1991 Unfolded optical glory of spheroids: backscattering of laser light from freely rising spheroidal air bubbles in water *Appl. Opt.* **30** 3429–42
[18] Zhang X *et al* 2002 The volume scattering function of natural bubble populations *Limnol. Oceanogr.* **47** 1273–82
[19] Monahan E C and Niocaill G M (ed) 1986 *Oceanic Whitecaps and Their Role in Air–Sea Exchange Processes* (Dordrecht: Reidel)
[20] Mishchenko M *et al* 2002 *Scattering, Absorption, and Emission of Light by Small Particles* (New York: Academic)